processes

MDPI

Article

Optimization of Drilling Parameters in Influence Area of Gas–Solid Interaction during Parallel Drilling Hole

Fengyan Zhang and Haidong Wang *

School of Mine Safety, North China Institute of Science and Technology, Langfang 111104, China; zfycumtb@163.com
* Correspondence: cytyzxn1000@163.com

Abstract: Previous studies have established that the selection of gas extraction borehole parameters is crucial for the effectiveness of gas extraction. To more accurately determine the reasonable extraction radius of gas extraction boreholes in the coal seam, this study was based on the actual occurrence conditions of the coal body. A coal-seam gas-seepage model, considering dynamic changes in permeability under gas–solid coupling conditions, was constructed. It was combined with FLAC^{3D} numerical simulations to develop a borehole extraction model closer to the field's natural needs. The study revealed the influence of borehole diameter and spacing on gas extraction, obtained the radius of effect of borehole extraction, and optimized the gas extraction borehole parameters based on data simulation experiments. Multiple sets of experimental results indicated that the optimal parameters are a borehole diameter of φ = 113 mm and a borehole spacing of 5 m. Applying these parameters in on-site tests at the 14,303 working faces of a particular mine significantly improved gas extraction efficiency, with a 29.7% increase in gas extraction concentration. This verified the accuracy of the simulation results and provides a scientific basis for cost reduction and efficiency enhancement in wellbore mining.

Keywords: gas extraction; directional boreholes; drilling parameters; permeability; numerical simulation

Citation: Zhang, F.; Wang, H. Optimization of Drilling Parameters in Influence Area of Gas–Solid Interaction during Parallel Drilling Hole. *Processes* **2023**, *11*, 2371. https://doi.org/10.3390/pr11082371

Academic Editor: Chin-Hyung Lee

Received: 14 June 2023
Revised: 31 July 2023
Accepted: 1 August 2023
Published: 7 August 2023

1. Introduction

Coal resources are pivotal to providing fundamental energy support for a country's social and industrial development, and thus occupy a critical strategic position [1–3]. They are essential for power consumption in various industries, including building materials, electric power, metallurgy, and other sectors relevant to people's livelihoods. Furthermore, coal is a vital energy source for supporting the metallurgical, chemical, iron, and steel industries, contributing significantly to the national economy [4–9]. With China being a major consumer of coal resources, its total energy consumption in 2022 witnessed a 2.9% increase compared to 2021, with coal's proportion rising by 0.2 percentage points and its growth rate accelerating by 4.3 percentage points [10]. As the nation's economy gradually recovers, the demand for coal rises, leading to a transition from shallow to deep mining of coal resources [11]. However, this shift presents challenges due to varying coal-forming environments, exposing coal mines to complex conditions like high ground stress, elevated temperatures, and concentrated gases, thereby increasing the risk of gas outbursts during mining operations [12,13].

Gas extraction from mines assumes great significance as a crucial hazard management approach in coal mining, ensuring the safe production of coal mines and protecting the operational safety of underground workers while promoting the development and utilization of coalbed methane resources [14]. Coal mines mainly use borehole extraction to effectively manage underground coalbed methane disasters [15,16]. In order to improve extraction efficiency, scholars have used numerous methods: the use of hydraulic fracturing [17], the use of carbon dioxide [18,19] or water [20] to drive out the gas, the nature of

the coal seam, or the stress. Nevertheless, the arrangement of extraction boreholes significantly influences the effectiveness of underground gas management. Improper extraction spacing, either too large or too small, can lead to suboptimal gas management, resulting in the inefficient use of resources [21]. Thus, setting reasonable parameters for arranging underground gas extraction boreholes is paramount.

Numerous scholars at home and abroad have undertaken extensive research and developed diverse numerical simulation methods to optimize the technical process of underground gas extraction borehole arrangement [22–25]. For instance, Motie et al. conducted CWI experiments on reservoir cores with varying wettability, proposing the SMB modeling procedure to study key parameters like permeability and the influence of CO_2 content on oil recovery [23]. Gutiérrez et al. combined hydraulic fracturing simulations with reservoir simulations using the 3D hydraulic fracturing simulator "HFWVU", investigating proppant transport, subsidence, fracture geometry changes, and expansion patterns [26]. Moreover, Abolfazl Abdollahipour et al. utilized a unique elemental model to determine fracture opening displacement, validated it through exact solutions, and performed a multi-parameter regression to consider the influence of surrounding pressure, rock properties, and fluid pressure and derive a mathematical model accounting for surrounding pressure effects [25]. Extensive studies on the arrangement of gas extraction boreholes have been conducted, addressing factors such as extraction radius and spacing relationships through numerical calculations [27–30]. Additionally, Shi established a mathematical model of coal-rock gas flow–solid coupling under multiple gravity effects, determining the extraction range of boreholes influenced by starting pressure in a coal mine [31]. Furthermore, Yan developed a logarithmic function based on the coupled gas–solid model of gas extraction, facilitating the determination of the optimal extraction radius [32]. Wang combined a numerical simulation with field tests, deriving reasonable parameters for long boreholes in cascade gas extraction [33].

In conclusion, numerous scholars have made significant research achievements in studying drilling parameter calculation models [34,35]. However, there has been relatively limited research on the impact of dynamic changes in permeability on coal-seam gas migration. Therefore, this paper aimed to develop a simulation model for gas extraction through directional boreholes that better represents actual field conditions and facilitates the optimization of drilling parameters. The proposed model is based on the theory of gas–solid coupling, incorporating principles from seepage mechanics and elastoplastic mechanics to account for dynamic changes in permeability. The $FLAC^{3D}$ 6.0 numerical simulation software simulated the gas extraction process from the coal seam using directional boreholes. Optimal drilling parameters were determined by analyzing plasticity, stress, and enhanced permeability zone distribution patterns during gas extraction with different borehole radii. A numerical simulation of down-hole extraction was presented.

2. Experimental Methods

2.1. Geometric Model and Parameters

Based on the site condition of a 14,301 working face in a mine, numerical simulation experiments were used to analyze the stress distribution pattern around the borehole based on the actual coal-seam physical and mechanical parameters and to explore the influence of the optimum borehole radius with extreme coupling. The experimental mechanical parameters are shown in Table 1.

Table 1. Mechanical parameters of the rock mass.

Formation Number	Density Kg/m^3	Bulk Modulus K/Gpa	Shear Modulus G/Gpa	Cohesion C/Mpa	Internal Friction Angle Φ (°)	Tensile Strength σ/Mpa
14 coal seam	1850	1.65	0.31	0.52	17.5	0.145

Through the influence range of the extraction borehole studied by many scholars, the size of the simulation model was determined, and a 3D simulation model with a geometry of 25 m × 20 m × 5 m was constructed, as shown in Figure 1.

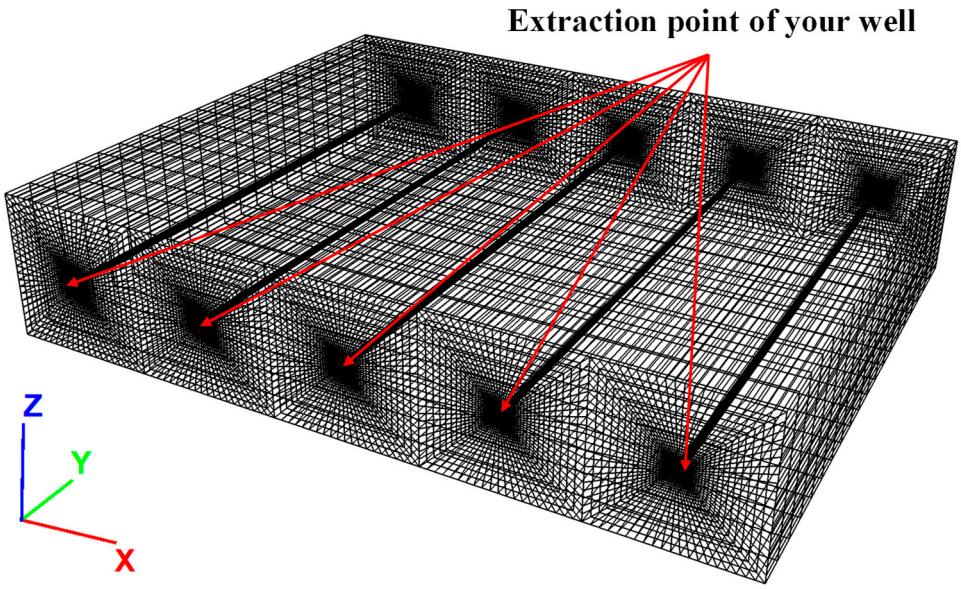

Figure 1. Three-dimensional simulation model.

The model grid density is divided in a non-homogeneous way. The thickness of model cells is negatively correlated with the distance from the borehole, with 208,000 structural cells and 216,741 calculation nodes, and the spacing between extraction boreholes is 5 m. The negative *Z*-axis pressure is set at the upper boundary of the simulated model, and the value is equal to the vertical stress of the overlying rock column. Due to the need to consider factors such as the influence of the extraction zone during the excavation of drill holes, displacement restriction conditions are imposed around and at the bottom of the model without affecting the balance of stress conditions at the base of the model. The boundary conditions and initial stress balance parameters are shown in Figure 2.

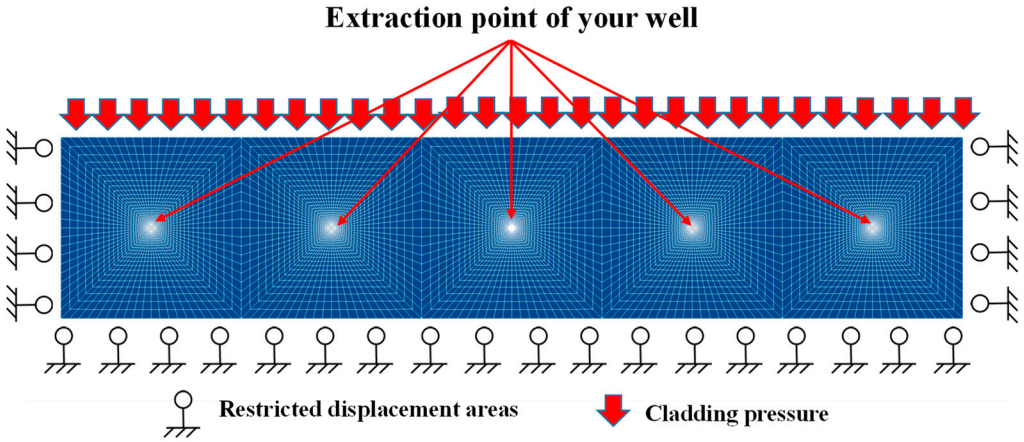

Figure 2. Boundary conditions and initial stress balance parameter.

2.2. Mathematical Model for Coal Seepage of Gas

During the construction of the cis borehole, the stresses and strains gradually increase, and the coal body around the borehole starts to slowly change from elastic deformation to plastic deformation and crushing deformation, increasing the permeability of part of the

coal seam. The damage criterion of the structural unit adopts the Mohr–Coulomb strength damage criterion as the primary yield criterion, namely:

$$F = \sigma_1 - \sigma_3 \frac{1 + \sin\varphi}{1 - \sin\varphi} \geq f_\theta \tag{1}$$

In Equation (1), F is the shear stress (MPa), σ_1 is the maximum principal stress (MPa), σ_3 is the minimum principal stress (MPa), φ is the angle of internal friction (°) and f_θ is the compressive strength (MPa).

Equation (2) is an expression for Coulomb's intensity criterion:

$$\sigma_1 = \frac{1 + \sin\varphi}{1 - \sin\varphi}\sigma_3 + \frac{2C + \cos\varphi}{1 - \sin\varphi} \tag{2}$$

The Mohr–Coulomb criterion allows for the refinement of the extended solid unit stress and strain components. The principal stress can be equivalently substituted into three stresses: σ_1, σ_2, and σ_3, representing the principal stress vector in the solid structural unit. The strain can be divided into strain components on the coordinate system: ε_1, ε_2, and ε_3. The coal-body stress variables obey the following laws, and the incremental expressions are shown in Equations (3)–(5).

$$\Delta\sigma_1 = \alpha_1\Delta\varepsilon_1^{\mathrm{e}} + \alpha_2(\Delta\varepsilon_2^{\mathrm{e}} + \Delta\varepsilon_3^{\mathrm{e}}) \tag{3}$$

$$\Delta\sigma_2 = \alpha_1\Delta\varepsilon_2^{\mathrm{e}} + \alpha_2(\Delta\varepsilon_1^{\mathrm{e}} + \Delta\varepsilon_3^{\mathrm{e}}) \tag{4}$$

$$\Delta\sigma_3 = \alpha_1\Delta\varepsilon_3^{\mathrm{e}} + \alpha_2(\Delta\varepsilon_1^{\mathrm{e}} + \Delta\varepsilon_2^{\mathrm{e}}) \tag{5}$$

In Equations (3)–(5), α_1 is the shear modulus G; α_2 is the bulk modulus K; $\Delta\varepsilon_1^{e}$ $\Delta\varepsilon_2^{e}$ $\Delta\varepsilon_3^{e}$ is the incremental modulus of elasticity in that direction (MPa);

In this numerical simulation test, the Mohr–Coulomb intrinsic model with the generalized linear elastic model as the base model and the introduction of the dynamic permeability parameter can provide the expressions for the basis of the stress variables derived from the strain tensor calculations for the solid structural units in the numerical simulation test.

The shear plastic flow function h^s and the tensile plastic flow function h^t quantitatively characterize the specific computational model. The shear plastic flow function h^s and the tensile plastic flow function h^t quantitatively characterize the specific computational model. The function h^s conforms to the non-association law and has the following expressions:

$$h^s = \sigma_1 - \sigma_3 N_\phi \tag{6}$$

$$N_\phi = \frac{1 + \sin\psi}{1 - \sin\psi} \tag{7}$$

In Equation (7), ψ is the angle of shear expansion, °.

When gas is extracted, the gas in the coal seam is transported through various fracture environments. The Darcy equation and Fick's law can express the equation of motion for gas through fractures and pores. The continuous flow of gas in the coal body from regions of high-ground stress to regions of low-ground stress is consistent with the generalized Darcy equation, which can be derived as follows:

$$Q_a = \frac{\partial m}{\partial t} - \Delta\left(\rho\frac{k}{\mu}\Delta p\right) \tag{8}$$

In Equation (8), Q_a is the coal-body gas transport, kg/(m^3·s); k is the coal-body permeability, md; μ is the model dynamic viscosity coefficient, Pa·s; ρ is the density of gas in the coal body, kg/m; p is the coal-seam gas pressure, Mpa.

Assuming that all the gas in the coal body is in the fracture-pore space, it can be concluded that the total mass of gas in the coal seam can be quantitatively characterized by the Langmuir equation, which is expressed as:

$$m = \rho_s \frac{V_L P}{L + P} + \rho_a \frac{V_L P}{P} + \phi \frac{MP}{RT} v \tag{9}$$

In Equation (9), m is the total mass of gas in the coal seam, kg; ρ_s is the apparent density of the industrial analysis coal body, kg/m^3; V_L is the Langmuir volume parameter, m^3/t; ϕ is the porosity of the coal body, %; M is the molecular weight of the gas, kg/mol; R is the gas parameter at standard conditions, J/(mol·K); T is the ideal experimental temperature, K; v is the volume of the coal seam, m^3.

The experiments assume a seepage boundary for gas transport in the media, i.e., there is no gas flow within the unit when the gas transport within the coal unit Q_a is 0. The gas flow control equation can be derived from Equations (8) and (9) as shown in Equation (10):

$$Q_a + \Delta\left(\rho \frac{k}{\mu} \Delta p\right) = \left(\rho_s \frac{V_L P}{(L + P)^2} + \rho_a \frac{V_L P}{p^2} + \phi \frac{M}{RT}\right) \frac{\partial p}{\partial t} + p \frac{M}{RT} \frac{\partial \phi}{\partial t} \tag{10}$$

This control equation is written into the initial Mohr–Coulomb intrinsic model fluid calculation module of FLAC^{3D} numerical simulation software to improve the accuracy of gas–solid coupling calculation for simulation experiments.

$$\begin{cases} \dfrac{\frac{\xi\gamma^{\rho^a}+\gamma^{\rho}}{\gamma^{\rho^a}} \exp\left[3\alpha\Delta\rho C_f + \frac{K\varepsilon_1 LC_f}{(L+P)^2} - C_f(\sigma_1+\sigma_{2+}\sigma_3)\right]}{k_a}, \gamma^{\rho^a} \geq \gamma^{\rho} \\ \dfrac{\xi \exp\left[3\alpha\Delta\rho C_f + \frac{K\varepsilon_1 LC_f}{(L+P)^2} - C_f(\sigma_1+\sigma_{2+}\sigma_3)\right]}{k_a}, \gamma^{\rho^a} \leq \gamma^{\rho} \end{cases} \tag{11}$$

At the same time, this calculation module needs to write the permeability and porosity, Equations (1) and (2) can characterize the stress of the coal seam, analyze Equation (4) with Equations (1) and (2), combine the coal-body elastic–plastic deformation theory and the original calculation equation of permeability, and derive the permeability dynamic change model as shown in Equation (11):

In Equation (11), k_a is the initial permeability of the calculated model, mD; γ^{ρ} is the value of plastic strain in the calculated model; γ^{ρ^a} is the initial value of plastic strain in the calculated model; C_f is the fracture compression coefficient; $\Delta\rho$ is the incremental gas pressure in the calculated model, MPa; ε_1 is the ultimate adsorption expansion deformation of the coal body (which must not be zero in the simulation).

Equation (11) will be written simultaneously into the simulation calculation module to eliminate the initial quantitative calculation equation.

The expressions for the coal-seam gas stress variables and the gas content equation under drilling and extraction conditions are coupled to produce a coal-seam gas-seepage model that considers the dynamic changes in coal-seam permeability under drilling and extraction conditions as follows:

$$\beta\left[\frac{2\varphi p}{p_a} + \frac{(1-\varphi)p^2}{Ep_a} + \frac{2bpb'}{L+P} - \frac{bb'p^2}{(L+P)^2}\right]\frac{\partial p}{\partial t} = -\frac{\alpha\beta p^2}{p_a}\frac{\partial \varepsilon}{\partial t} \tag{12}$$

In Equation (12), E is the bulk modulus of elasticity of the gas-bearing coal body, Pa; α is the influential stress factor of Biot; β is the stress influence (coupling) factor, and ε is the bulk strain of the gas-bearing coal body.

Equation (12) is applied to replace the gas–solid coupling control module in FLAC^{3D} software and applied jointly with the fluid calculation module of the intrinsic model constructed above to invert the real distribution characteristics of gas–solid coupling on the shaping region, the principal stress and the seepage increase region during gas extraction.

3. Analysis of Numerical Simulation Results

After the initial mechanical equilibrium, the gas extraction simulation experiments were carried out under different borehole diameters, with data recording points arranged sequentially along the positive *X*-axis at 0.125 m and cloud slice analysis locations along the *Y*-axis at an interval of 2.5 m. The variables of each experimental group are shown in Table 2.

Table 2. Variables for each experimental group.

No.	Hole Diameter φ/mm	Hole Spacing m
1	93	5
2	113	5
3	153	5
4	93	10
5	113	10
6	153	10

3.1. Model Validation

To verify the reasonableness of the gas–solid coupling model, this paper simulated and analyses the variation of gas extraction flow rate within 30 d with and without the gas–solid coupling model and fits it to the monitoring data of a 14,303 working face to verify the results. As can be seen from Figure 3, the gas extraction flow rate variation law using the gas–solid coupling model matches the field monitoring data to a high degree, and the data range is more compatible. In contrast, the extraction flow rate without the gas–solid coupling model is lower than the field data. This shows that the model constructed in this paper is reasonable and accurate and can be used to predict the actual extraction situation and optimize the drill-hole layout parameters.

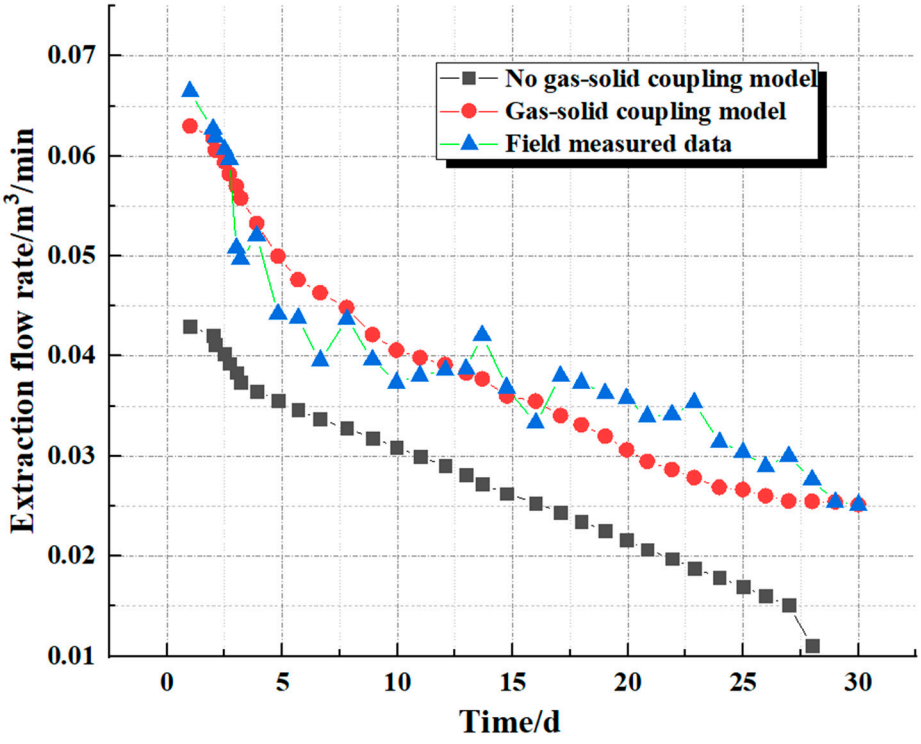

Figure 3. Graph matching results of simulated and field monitoring data.

3.2. Characteristics of the Distribution of the Plastic Zone of the Coal Body around the Extraction Borehole

To investigate the influence range of gas extraction under different hole diameter conditions, the simulation experiment selected the extraction borehole's vertical direction (Y-axis direction) as the cross-section. It analyzed the distribution characteristics of the coal elasticity area around the borehole when the diameter φ is 93 mm, 113 mm, and 153 mm. The simulation results are shown in Figure 4.

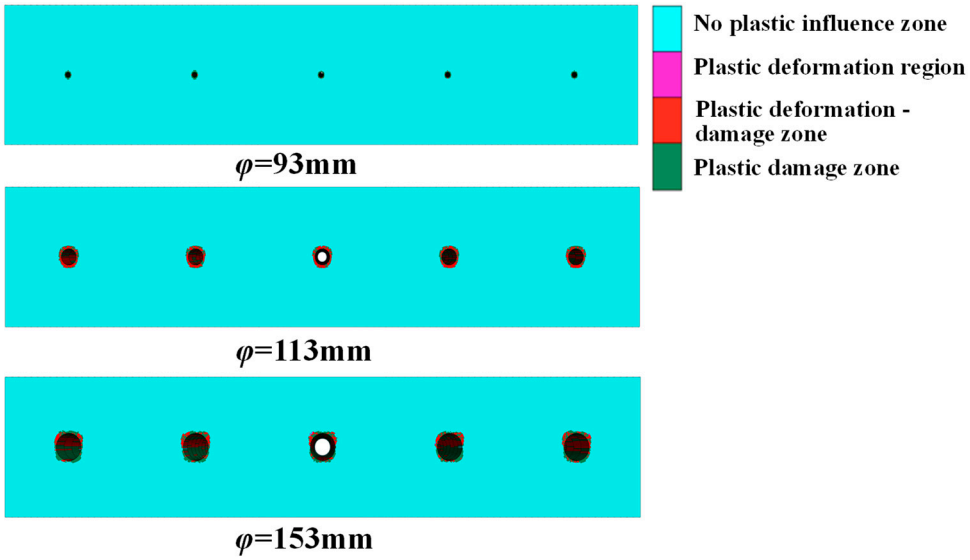

Figure 4. Distribution characteristics of plastic areas with different pore sizes.

The plastic zone of the coal body is a crucial factor for the effective release of coal-seam fracture expansion during the extraction process. As shown in Figure 4, the borehole radius and distance from the borehole influence the plastic zone area. For instance, when the borehole diameter is slight, such as 93 mm, the plastic zone around the borehole is too small to effectively release the coal-seam fracture expansion, limiting the efficiency of the extraction process. Conversely, when the borehole diameter increases to 113 mm, the area of the plastic zone of the coal body around the borehole increases and expands evenly in all directions. This leads to a more effective release of the coal-seam fracture expansion and improved extraction efficiency. However, when the borehole diameter reaches 153 mm, the plastic zone of the coal body around the borehole reaches its maximum size, and the growth rate of the plastic zone decreases. This increases the deformation of the surrounding rock, which generates more fractures around the borehole, leading to an increase in the permeability and porosity of the coal seam. Although the permeability and porosity of the coal seam are increased, the deformation of the surrounding rock increases, which can lead to instability in the extraction area. It is shown that the size of the plastic zone in the coal body around the borehole is positively correlated with the borehole's radius and that the plastic zone's expansion is necessary for effective seam fracture extension. However, a balance must be struck between plastic zone extension and surrounding rock deformation to ensure efficient mining without compromising stability. The simulation results are shown in Figure 5.

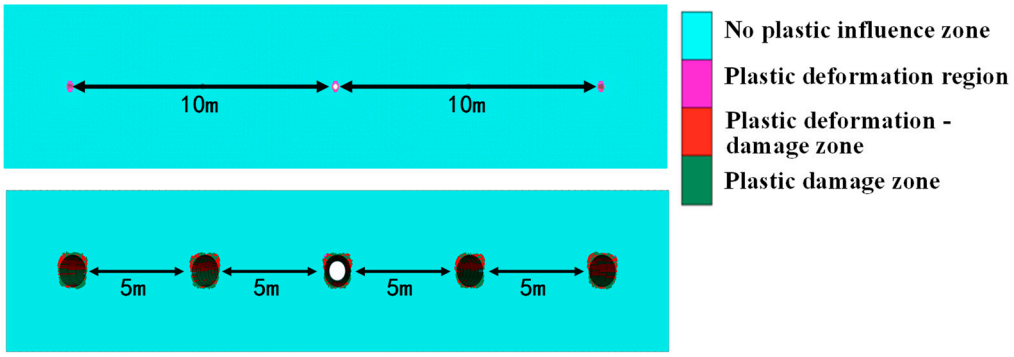

Figure 5. Characteristics of the distribution of plastic zones at different borehole spacings.

As can be seen from Figure 5, as the spacing decreases, the number of boreholes in the same area of the seam increases, the area of plastic damage gradually expands and connects, and the total area of damage increases, with a plastic damage area of 1.9 m^2 at a spacing of 10 m, increasing to 10.2 m^2 after the spacing is reduced to 5 m, an increase of 5.36 times. As the spacing of the boreholes decreases, the number of boreholes in the same area increases, which results in a gradual expansion and linking of the plastic damage area and a growth in the total damage area. This is because the boreholes serve not only to discharge gas but also to reduce the stress concentration within the seam and slow down the formation of stress concentration zones, thus reducing the extent of damage to the hem. In addition, as the spacing between boreholes decreases, the distance between boreholes becomes shorter, which means that the fractures within the seam are more developed, and the permeability increases accordingly.

3.3. Characteristics of the Main Stress Distribution in the Coal Body around the Extraction Borehole

The characteristics of the main stress distribution in the surrounding coal body with drilling hole diameters of φ = 93 mm, 113 mm, and 153 mm are shown in Figure 6.

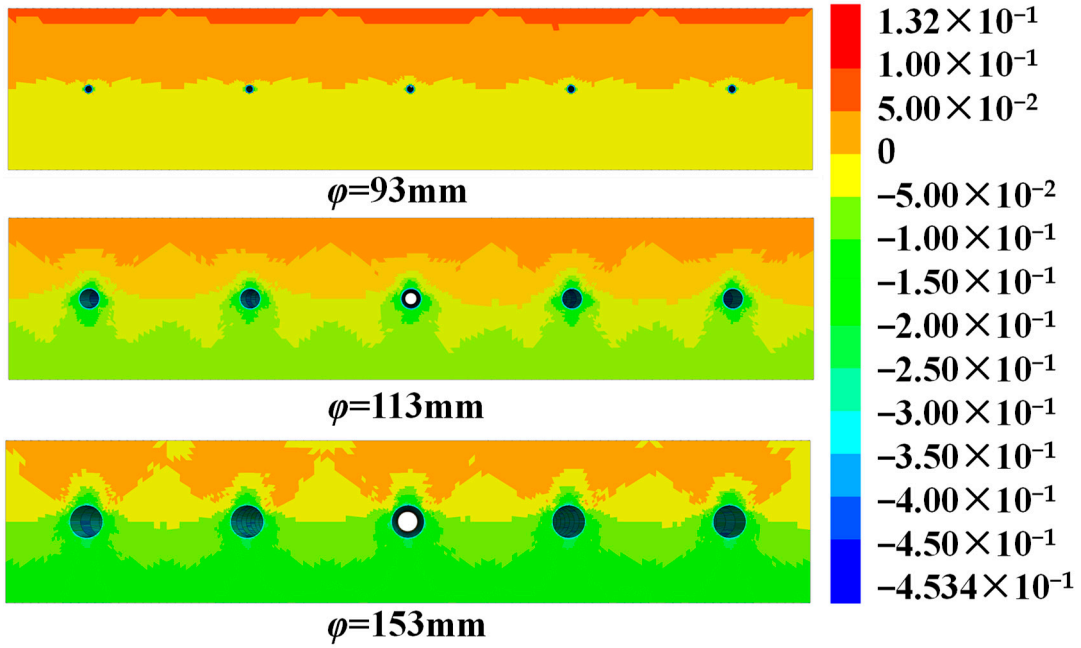

Figure 6. Characteristics of the main stress distribution for different bore sizes.

The relationship between borehole diameter and stress unloading area is an essential factor affecting the extraction efficiency of underground coal mines. As shown in Figure 6,

with the gradual increase of borehole diameter, the stress unloading area gradually increases, and the regional distribution features change from circular-like to elliptical-like, and finally show an "X" type distribution state. In addition, the stress unloading area gradually connects and unloads the upper coal-seam ground stress. However, when the borehole diameter $\varphi = 153$ mm, the unloading range is smaller than that of $\varphi = 113$ mm, with a peak stress value of 0.241 MPa, as shown in Figure 7. Furthermore, the stress unloading area increases due to the excessive influence of extraction. However, the stress is not entirely unloaded in some areas around the borehole due to stress-compound areas, resulting in the stress concentration phenomenon. The stress concentration in some areas around the borehole may increase the risk of collapse of the borehole. It should be noted that the stress concentration and unloading area are also affected by the depth of the borehole and the geological structure of the coal seam. Therefore, choosing an appropriate borehole diameter and layout is important to effectively unload the ground stress and reduce the risk of borehole collapse. Moreover, the relationship between the borehole diameter and stress unloading area also affects the permeability and porosity of the coal seam. As shown in Figure 4, the plastic zone of the coal body around the borehole is positively correlated with the borehole radius. When the borehole diameter is increased to φ = 153 mm, the area of the plastic zone of the coal body around the borehole is the largest, causing an increase in the permeability and porosity of the coal seam. It shows that the relationship between the borehole diameter and stress unloading zone is an important factor affecting the efficiency and safety of underground coal mining. A suitable borehole diameter and layout can effectively unload ground stresses, increase the permeability and porosity of the coal seam, and reduce the risk of borehole collapse.

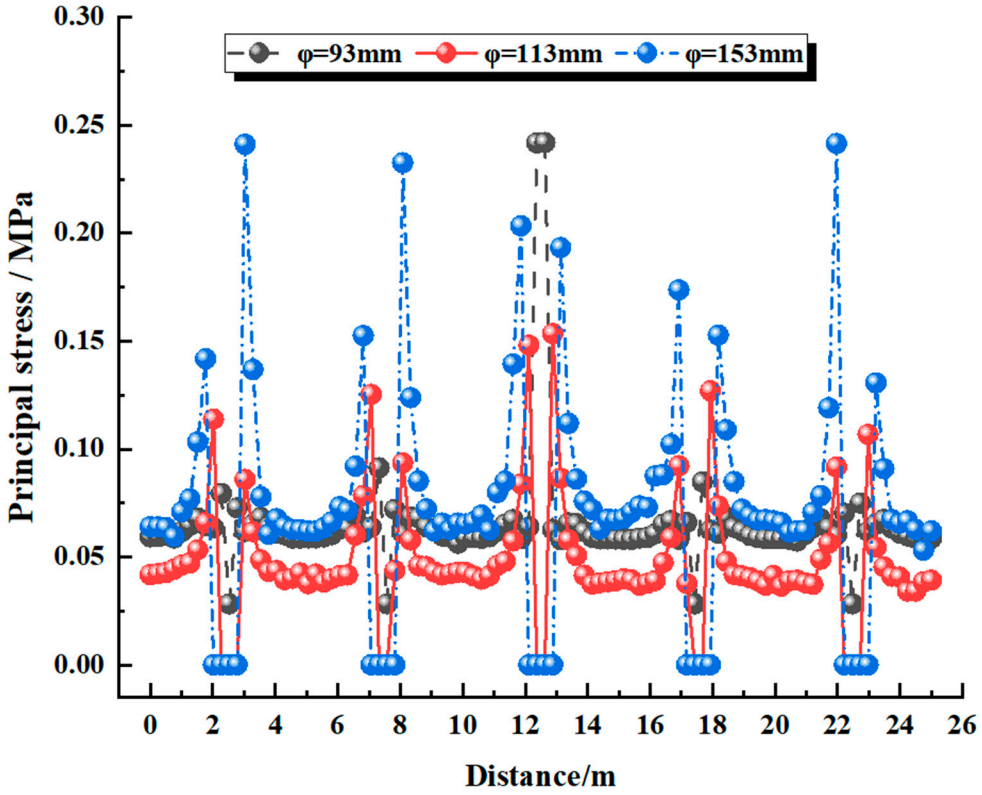

Figure 7. The plot of main stress distribution for different bore sizes.

The simulated results are shown in Figure 8, which analyses the characteristics of the main stress distribution around the coal body when the drill-hole spacing is 5 m and 10 m.

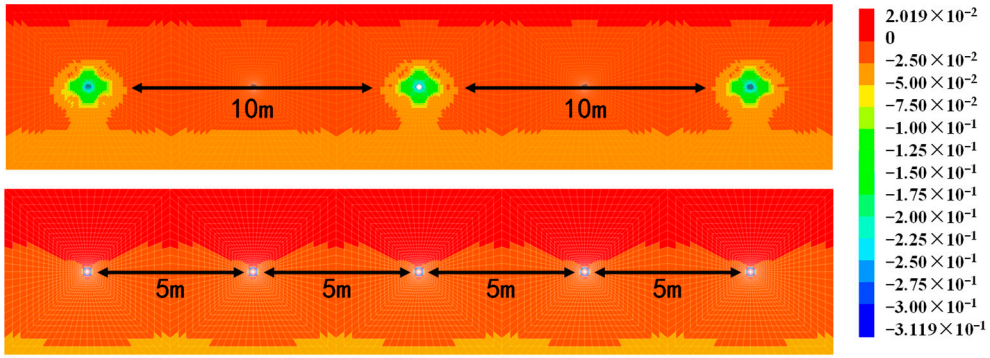

Figure 8. Characteristics of principal stress distribution for different borehole spacing.

The spacing between drill holes plays a significant role in the overall influence of the drill-hole arrangement area. As drill-hole spacing increases, the stress influence range of a single drill hole also increases, and the overall influence range of the drill-hole arrangement area decreases. Figure 8 shows that when the drill-hole spacing is 10 m, a significant portion of the area between drill holes is unaffected, and the influence area of drill holes develops mainly towards the top and bottom of the coal seam. However, as the construction of drill holes alters the original equilibrium of the coal body, some of the stresses are transferred to the unaffected area between drill holes. In addition, the extraction area of drill holes may not effectively reach the deep part of the coal seam, which may lead to dangerous stress concentration areas. On the other hand, when the drill-hole spacing is 5 m, a smaller portion of the area between drill holes is unaffected, but the unaffected area is still significant compared to the drill-hole spacing of 2 m. Moreover, as the drill-hole spacing is smaller, the influence area of drill holes develops mainly towards the middle of the coal seam, which reduces the stress concentration area and increases the gas extraction efficiency. In summary, the drill-hole spacing should be determined based on the geological conditions and the characteristics of the coal seam. A larger drill-hole spacing may reduce the overall influence of the drill-hole arrangement area but also increase the risk of stress concentration areas. Conversely, a smaller drill-hole spacing may increase the influence of drill holes on the coal seam, but it may also improve the gas extraction efficiency and reduce the risk of stress concentration areas. Therefore, carefully considering these factors should determine the optimal drill-hole spacing.

3.4. Characteristics of the Distribution of Seepage Enhancement Areas in the Coal Body around the Extraction Borehole

The seepage distribution pattern increases the coal body's area around the borehole when the borehole diameter φ is 93 mm, 113 mm, and 153 mm, as shown in Figure 9.

Figure 9 illustrates that the size of the seepage zone is closely related to the diameter of the borehole. The larger the borehole diameter, the larger the seepage zone. Additionally, the expansion trend of the seepage zone is consistent with that of the stress unloading zone. Furthermore, the permeability of the coal body between the boreholes gradually increases. When a 153 mm borehole diameter is used for gas extraction, the permeability zone continues to increase with the gradual increase of the borehole diameter. This expansion generates a compound influence zone, creating numerous fissures through the joint action of the double boreholes. As a result, gas leaks directly into the working face via the fissures. However, this scenario means that the extraction borehole needs to be able to extract gas from this area effectively.

The increase in borehole diameter leads to an increase in the extent of plastic disruption, resulting in the expansion of fracture development in the coal rock surrounding the borehole. This expansion leads to an increase in coal-rock permeability values. However, as the borehole diameter increases, the seepage zone also increases, and eventually, the compound influence zone and the stress unloading zone exceed the range of the extraction borehole. Thus, it becomes difficult to extract gas from this area.

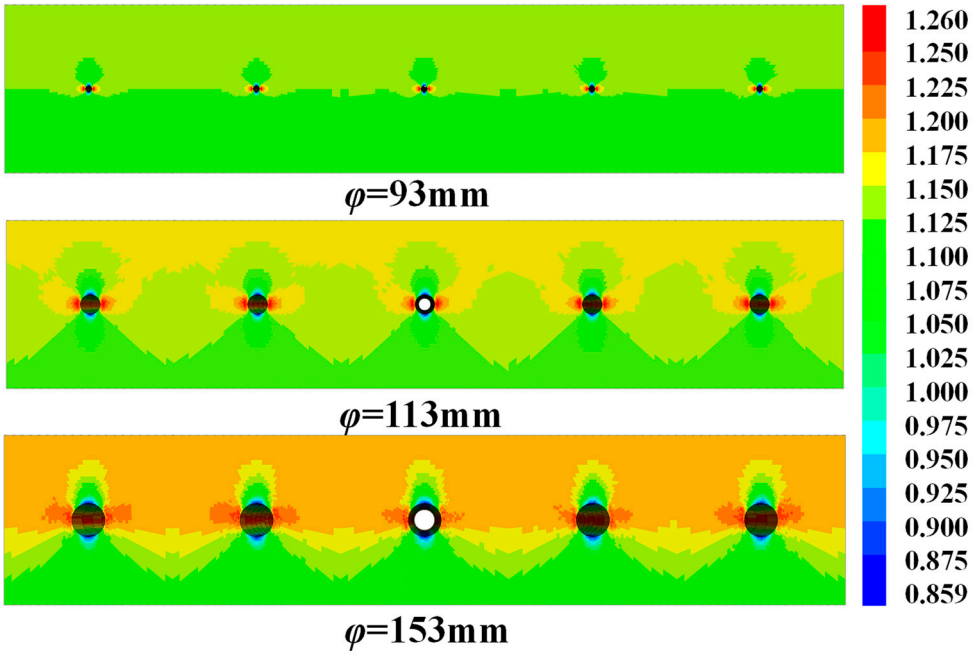

Figure 9. Characteristics of the distribution of seepage enhancement areas with different pore sizes.

Therefore, choosing the appropriate borehole diameter is necessary to ensure effective gas extraction. There may be better choices than using a borehole diameter of 153 mm for gas extraction due to the potential for fissure development and the consequent failure to extract gas effectively. Instead, it is necessary to balance the increase in permeability with the expansion of the seepage zone and select an appropriate borehole diameter to maximize gas extraction efficiency without compromising safety.

The effect of borehole diameter on coal-rock permeability was analyzed in this study, and the results are presented in Figure 10. The graph clearly shows that the permeability of the coal body reaches a maximum at the borehole layout and decreases rapidly with distance from the borehole. Interestingly, as the borehole diameter gradually increased, the permeability near the borehole increased significantly. The peak permeability values are 0.702 mD in the 93 mm borehole, 1.411 mD in the 113 mm borehole, and 1.416 mD in the 153 mm borehole, representing a maximum increase of 48%. The increase in coal-rock permeability values can be attributed to the expansion of fracture development in the borehole coal rock, which is caused by the extent of plastic disruption. This means that the plastic disruption caused by the borehole drilling process leads to the expansion of fractures in the surrounding coal rock, increasing permeability.

It is worth noting that although the peak permeability of the 153 mm borehole is higher than that of the 113 mm borehole, the increase in permeability is not proportional to the increase in borehole diameter. Therefore, selecting a larger borehole diameter may only sometimes result in a significant increase in permeability. This study provides valuable insights into the relationship between the borehole diameter and coal-rock permeability. The findings suggest that the extent of plastic disruption caused by borehole drilling can significantly impact the permeability of the coal rock and that selecting appropriate borehole diameters is crucial for optimizing gas extraction efficiency. The simulation results are shown in Figure 11.

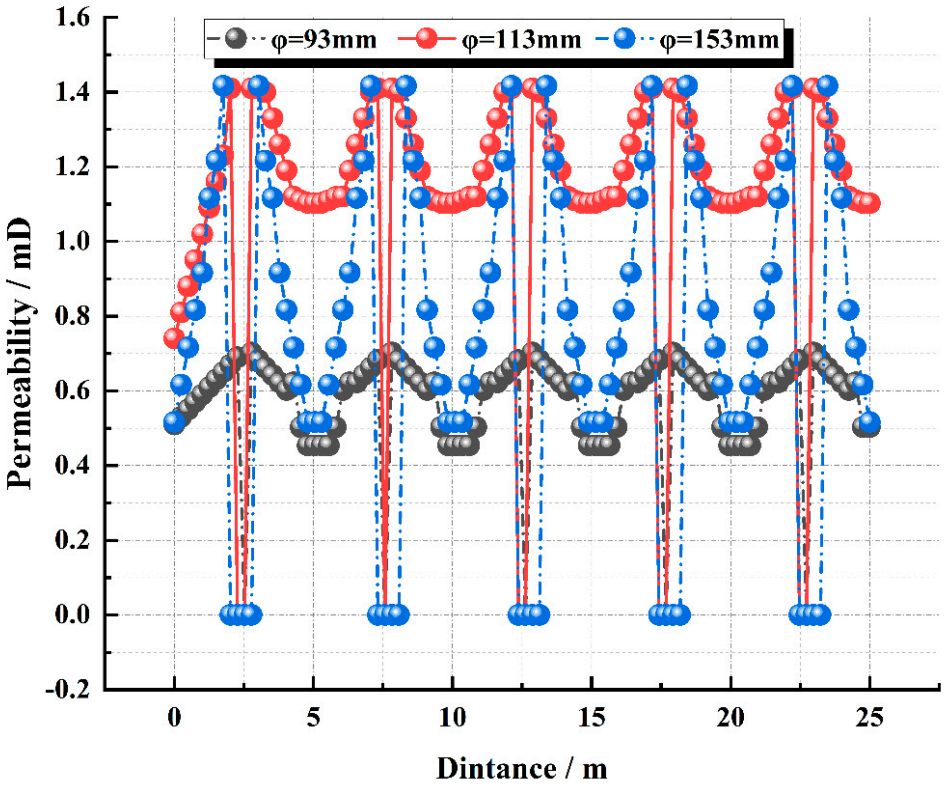

Figure 10. Variation in permeability for different pore sizes.

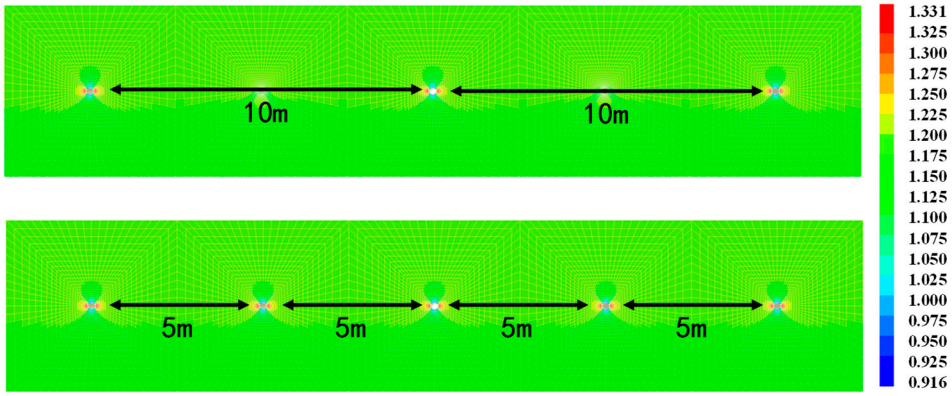

Figure 11. Characteristics of the distribution of seepage enhancement areas with different borehole spacing.

As can be seen from Figure 11, the permeability increases from 0.859 mD to 1.26 mD at 10 m drill-hole spacing, an increase of 9%; when the drill-hole spacing is reduced to 5 m, the permeability at the center point increases from the initial 0.915 mD to 1.331 mD, an increase of 45%. This is because the reduction of the drill-hole spacing aggravates the plastic destruction of the coal rock, the fracture development at the central point is higher, and the permeability increases; accordingly, as the extraction proceeds, the decay of the gas content shrinks the coal matrix, the fracture width expands further, so the permeability gradually increases, the smaller the spacing is, the more significant the increase in permeability. The smaller the spacing, the greater the increase in permeability. The shorter the spacing between boreholes, the more significant the plastic breakdown of the coal rock, the greater the fracture development at the center, and there is a corresponding increase in greater permeability.

As the extraction progresses, the decay of the gas content shrinks the coal matrix, and the fissure width expands further, leading to a gradual increase in permeability. As a result,

the fracture width increases more rapidly when the hole spacing is reduced, resulting in greater permeability.

By analyzing the stress, plasticity, and permeability increase zones under different extraction borehole sizes and considering the extraction effect and safety dimension, an extraction borehole size of 113 mm and a borehole spacing of 5 m was selected.

4. Engineering Application of Preferred Parameters and Investigation of Extraction Effects

4.1. Engineering Application Solutions

Based on the preferred results, the 14,303-working face of a mine was selected for field engineering application. The coal seam is a low-permeability seam with no extraordinary geological formations. Two groups of down-seam extraction boreholes are arranged in the test area in sequence, with a borehole diameter of 113 mm and a borehole spacing of 5 m in Group A, a borehole diameter r 113 m in Group 1–3, and a borehole diameter of 93 mm and borehole spacing 10 m in Group B, boreholes 4–6, as an object control group. The true gas extraction volume was calculated by recording and measuring the flow rate and concentration of gas extracted over a 30-day period.

4.2. Measured Results and Analysis

The continuous monitoring data in Figure 12 show the average gas extraction volume from the gas drainage boreholes over 30 days. Both Group A and Group B boreholes underwent 30 days of continuous extraction. For Group B boreholes, the gas extraction rate decreased from 0.0665 m^3/min to 0.0251 m^3/min, while for Group A boreholes, the rate decreased from 0.083 m^3/min to 0.0472 m^3/min. This resulted in a remarkable 29.7% increase in gas extraction efficiency.

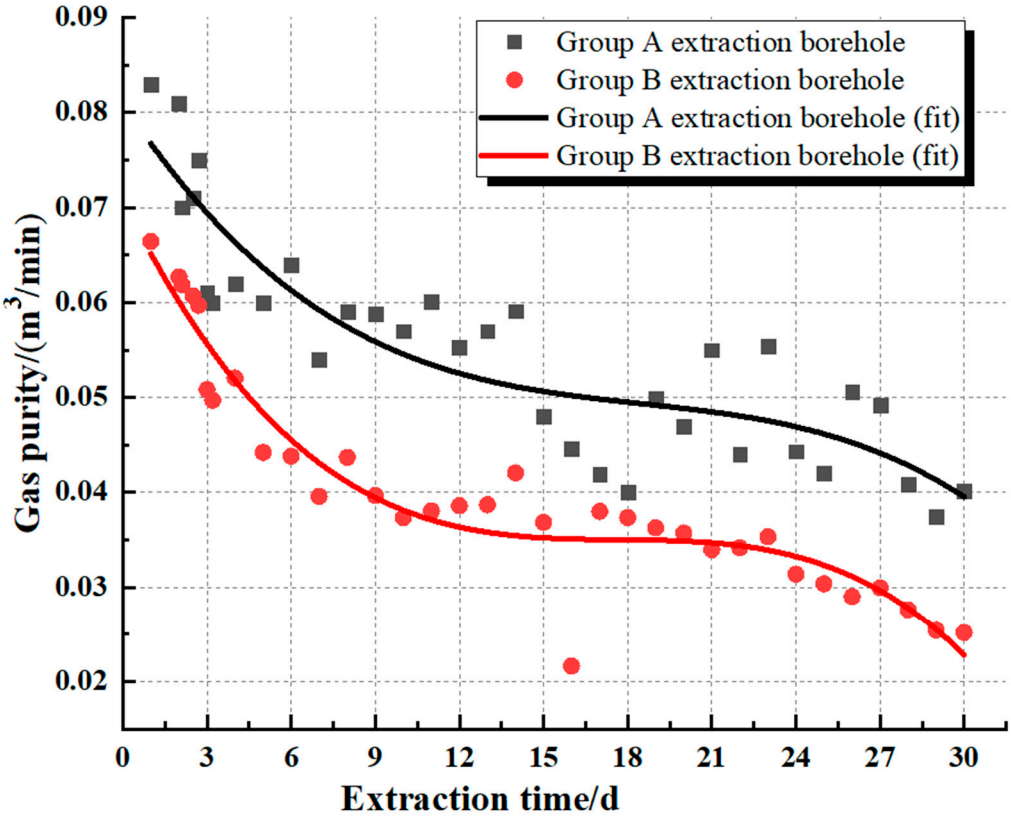

Figure 12. Comparison of pure gas extraction volumes for different boreholes.

The significant improvement in gas extraction efficiency underground and the positive impact on working conditions at the production face can be attributed to the judicious

selection of borehole radius and spacing. This study of continuous monitoring provides compelling evidence for optimizing gas extraction, and its implications are crucial for enhancing both underground safety and production efficiency.

5. Conclusions

(1) This passage is based on the geological conditions of a 14,301 working face in a mine. It combines the traditional gas–solid coupling model and gas migration theory to construct a coalbed methane seepage simulation model that considers the dynamic changes in coal-seam permeability. The model accurately reflects the mechanical evolution characteristics of surrounding coal during directional drilling and gas extraction;

(2) Incorporating the coalbed methane seepage simulation model, this study revealed the influence of borehole diameter and spacing on the gas–solid coupling zone. Numerical simulation experiments were conducted on the drilling and gas extraction process under various borehole diameters and spacing conditions. As a result, an optimal borehole diameter of 113 mm and a borehole spacing of 5 m were determined for gas extraction;

(3) The optimized parameters for gas extraction were implemented in a field-engineering practice, with a borehole diameter of 113 mm and a borehole spacing of 5 m. As a result, the methane extraction concentration increased by 29.7%, significantly increasing the on-site methane extraction rate. This improvement notably enhanced gas extraction efficiency and reduced the risk of coal and gas outbursts.

Author Contributions: Conceptualization, H.W.; data curation, F.Z.; writing—original draft preparation, F.Z.; writing—review and editing, F.Z.; visualization, H.W.; supervision, H.W. All authors have read and agreed to the published version of the manuscript.

Funding: This research is financially supported by the National Natural Science Foundation of China (Grant No. 52174077, No. 51774165).

Data Availability Statement: The data presented in this study are available on request from the corresponding author. The data are not publicly available due to some authors' personal privacy and legal restrictions.

Conflicts of Interest: The authors declare no conflict of interest.

Nomenclature

F	is the shear stress (MPa);
σ_1	is the maximum principal stress (MPa);
σ_3	is the minimum principal stress (MPa);
φ	is the angle of internal friction;
f_θ	is the compressive strength (MPa);
C	is the cohesion of the rock material (MPa);
α_1	is the shear modulus G;
α_2	is the bulk modulus K;
$\Delta\varepsilon_1^e$ $\Delta\varepsilon_2^e$ $\Delta\varepsilon_3^e$	is the incremental modulus of elasticity in that direction (MPa);
h^s	is The shear plastic flow function;
h^t	is the tensile plastic flow function;
ψ	is the angle of shear expansion, °;
Q_a	is the coal-body gas transport, kg/(m^3·s);
k	is the coal-body permeability, md;
μ	is the model dynamic viscosity coefficient, Pa·s;
ρ	is the density of gas in the coal body, kg/m;
p	is the coal-seam gas pressure, MPa;
m	is the total mass of gas in the coal seam, kg;
ρ_s	is the apparent density of the industrial analysis coal body, kg/m^3;
V_L	is the Langmuir volume parameter, m^3/t;
ϕ	is the porosity of the coal body, %;
M	is the molecular weight of the gas, kg/mol;
R	is the gas parameter at standard conditions, J/(mol·K);

T	is the ideal experimental temperature, K;
v	is the volume of the coal seam, m^3;
k_a	is the initial permeability of the calculated model, mD;
γ^{ρ}	is the value of plastic strain in the calculated model;
γ^{ρ^a}	is the initial value of plastic strain in the calculated model;
C_f	is the fracture compression coefficient;
$\Delta\rho$	is the incremental gas pressure in the calculated model, MPa;
ε_1	is the ultimate adsorption expansion deformation of the coal body (which must not be zero in the simulation);
E	is the bulk modulus of elasticity of the gas-bearing coal body, Pa;
α	is the effective stress factor of Biot;
β	is the stress influence (coupling) factor;
ε	is the bulk strain of the gas-bearing coal body.

References

1. Wang, K.; Guo, Y.; Du, F.; Dong, H.; Xu, C. Effect of the water injection pressure on coal permeability based on the pore-fracture fractal characteristics: An experimental study. *Greenh. Gases Sci. Technol.* **2021**, *12*, 136–147. [CrossRef]
2. Wang, K.; Guo, Y.; Xu, H.; Dong, H.; Du, F.; Huang, Q. Deformation and permeability evolution of coal during axial stress cyclic loading and unloading: An experimental study. *Geomech. Eng.* **2021**, *24*, 519–529. [CrossRef]
3. Liu, Z.; Yang, H.; Wang, W.; Cheng, W.; Xin, L. Experimental Study on the Pore Structure Fractals and Seepage Characteristics of a Coal Sample around a Borehole in Coal Seam Water Infusion. *Transp. Porous Media* **2018**, *125*, 289–309. [CrossRef]
4. Wang, K.; Guo, Y.; Wang, G.; Du, F. Seepage and Mechanical Failure Characteristics of Gas-bearing Composite Coal-Rock under True Triaxial Path. *J. China Coal Soc.* **2023**, 226–237. (In Chinese) [CrossRef]
5. Huang, H.; Zhao, J.; Xu, L.; Wang, K. Analysis of supply and demand relations of coal market in new period. *Chin. Coal* **2021**, *47*, 8–15. (In Chinese) [CrossRef]
6. Wang, Q. Under the double carbon target, it is difficult to change the main energy status of coal. *China Mining News*, 19 July 2021. [CrossRef]
7. Wang, G.; Guo, Y.; Wang, P.; Li, W.; Wu, M.; Sun, L.; Cao, J.; Du, C. A new experimental apparatus for sudden unloading of gas-bearing coal. *Bull. Eng. Geol. Environ.* **2020**, *79*, 857–868. [CrossRef]
8. Wang, S. Thinking about the main energy position of coal and green mining. *Chin. Coal* **2020**, *46*, 11–16. [CrossRef]
9. Zhang, H. The situation and task of coal industry 14th five-year plan development. *Bus. Obs.* **2020**, 56–60.
10. Jiang, M.R.; Xiao, X.J. Analysis of coal supply and demand situation in 2019 and outlook in 2020. *China Energy* **2020**, *42*, 9–13. (In Chinese)
11. Shi, S.; Zeng, M.; Li, H.; Lu, Y. Evolution and warning of coal spontaneous combustion and gas symbiotic dis-asters. *Coal Mine Saf.* **2022**, *53*, 9–16. (In Chinese) [CrossRef]
12. Zhou, Y. Analysis and application of gas control in deep coal seam mining. *Min. Equip.* **2022**, 50–52. (In Chinese) [CrossRef]
13. Jing, Z. Multi-source data fusion mine ventilation gas disaster warning platform. *Coal Technol.* **2022**, *41*, 237–239. (In Chinese) [CrossRef]
14. Liu, C.; Sun, D.; Wu, W.; Li, L.; Sun, Z. Technology system and prospect of advanced large-scale precision prevention and control of coal mine gas disaster in China. *Coal Geol. Explor.* **2022**, *50*, 82–92. (In Chinese)
15. Slastunov, S.; Kolikov, K.; Batugin, A.; Sadov, A.; Khautiev, A. Improvement of Intensive In-Seam Gas Drainage Technology at Kirova Mine in Kuznetsk Coal Basin. *Energies* **2022**, *15*, 1047. [CrossRef]
16. An, F.; Cheng, Y. The Effect of a Tectonic Stress Field on Coal and Gas Outbursts. *Sci. World J.* **2014**, *2014*, 813063. [CrossRef]
17. Li, Q.; Lu, Y.; Ge, Z.; Zhou, Z.; Zheng, J.; Xiao, S. A New Tree-Type Fracturing Method for Stimulating Coal Seam Gas Reservoirs. *Energies* **2017**, *10*, 1388. [CrossRef]
18. Álvarez-Fernández, M.-I.; Prendes-Gero, M.-B.; Peñas-Espinosa, J.-C.; González-Nicieza, C. Innovative Techniques in Underground Mining for the Prevention of Gas Dynamic Phenomena. *Energies* **2021**, *14*, 5205. [CrossRef]
19. Vishal, V.; Mahanta, B.; Pradhan, S.; Singh, T.; Ranjith, P. Simulation of CO_2 enhanced coalbed methane recovery in Jharia coal-fields, India. *Energy* **2018**, *159*, 1185–1194. [CrossRef]
20. Huang, B.; Lu, W.; Chen, S.; Zhao, X. Experimental investigation of the functional mechanism of methane displacement by water in the coal. *Adsorpt. Sci. Technol.* **2020**, *38*, 357–376. [CrossRef]
21. Kulikova, A.; Ovchinnikova, T. On the issue of reducing geoecological risks at mining enterprises. *Min. Informational Anal. Bull.* **2021**, *2*, 251–262. [CrossRef]
22. Salazar-Mendoza, R.; Garcia-Gutierrez, A. A Two-Region Hydraulic Averaging Model for Cuttings Transport during Horizontal Well Drilling. *J. Can. Pet. Technol.* **2008**, *47*, 55–61. [CrossRef]
23. Motie, M.; Assareh, M. CO_2 sequestration using carbonated water injection in depleted naturally fractured reservoirs: A simulation study. *Int. J. Greenh. Gas Control.* **2020**, *93*, 102893. [CrossRef]

24. García-Gutiérrez, A.; Martínez-Estrella, J.I.; Hernández-Ochoa, A.F.; Verma, M.P.; Mendoza-Covarrubias, A.; Ruiz-Lemus, A. Development of a numerical hydraulic model of the Los Azufres steam pipeline network. *Geothermics* **2009**, *38*, 313–325. [CrossRef]
25. Abdollahipour, A.; Marji, M.F.; Bafghi, A.Y.; Gholamnejad, J. DEM simulation of confining pressure effects on crack opening displacement in hydraulic fracturing. *Int. J. Min. Sci. Technol.* **2016**, *26*, 557–561. [CrossRef]
26. García-Gutiérrez, A.; Hernández, A.; Martínez, J.; Ceceñas, M.; Ovando, R.; Canchola, I. Hydraulic model and steam flow numerical simulation of the Cerro Prieto geothermal field, Mexico, pipeline network. *Appl. Therm. Eng.* **2015**, *75*, 1229–1243. [CrossRef]
27. Yan, W. Analysis of gas extraction effect of directional long borehole along bedding. *Coal Technol.* **2017**, *36*, 164–165. (In Chinese)
28. Shi, Z.; Gao, S. Optimization of large diameter high level gas extraction borehole layout on fully mechanized mining face. *Jiangxi Coal Sci. Technol.* **2023**, 153–155. (In Chinese)
29. Cui, P.; Chen, X.; Li, X.; Wang, M.; Zhang, J. Study on gas control technology of 4321 working face in chengzhuang mine. *Coal Technol.* **2022**, *41*, 143–147. (In Chinese) [CrossRef]
30. Lu, Y.; Shen, H.; Qin, B.; Zhang, L.; Ma, H.; Mao, T. Mahonfen and peach. Study on gas extraction radius and spacing of bedding borehole. *J. Min. Saf. Eng.* **2015**, *32*, 156–162. (In Chinese) [CrossRef]
31. Shi, Y.; Wang, Z.; Liang, B.; Zhou, Y.; Sun, W. Numerical simulation study on spacing of boreholes for pre-pumping gas in the bedding of coal seam. *China Saf. Prod. Sci. Technol.* **2017**, *13*, 21–27. (In Chinese)
32. Yan, F.; Yang, H. Numerical simulation of plastic influence radius of hydraulic cavitation along coal seam. *Coal Technol.* **2023**, *42*, 175–178. (In Chinese) [CrossRef]
33. Wang, Y.; Cai, F.; Zhao, Q.; Wang, Z. Simulation test of gas lift slagging in long borehole of gas extraction along strata. *Coal Mine Saf.* **2022**, *53*, 184–190. (In Chinese) [CrossRef]
34. Rybak, J.M.; Kongar-Syuryun, C.; Tyulyaeva, Y.; Khayrutdinov, A.M.; Akinshin, I. Geomechanical substantiation of parameters of technology for mining salt deposits with a backfill. *Min. Sci.* **2021**, *28*, 19–32. [CrossRef]
35. Khayrutdinov, M.; MISiS, N.; Kongar-Syuryun, C.; Tyulyaeva, Y. Improving Safety when Extracting Water-soluble Ores by Optimizing the Parameters of the Backfill Mass. *Occup. Saf. Ind.* **2021**, *2021*, 53–59. [CrossRef]